6
Non-Tensorial Properties

6.1
Strength Properties

If solid bodies are exposed to ever increasing mechanical stress, one normally observes, after a range of stress proportional deformation, an increase in deviations from Hooke's Law, whereby, all processes remain reversible. After further deformation one finds an increasing resistance (strain hardening) associated with irreversible deformation (plastic deformation) and finally breaking processes. Figure 6.1 presents such a behavior in tensile testing.

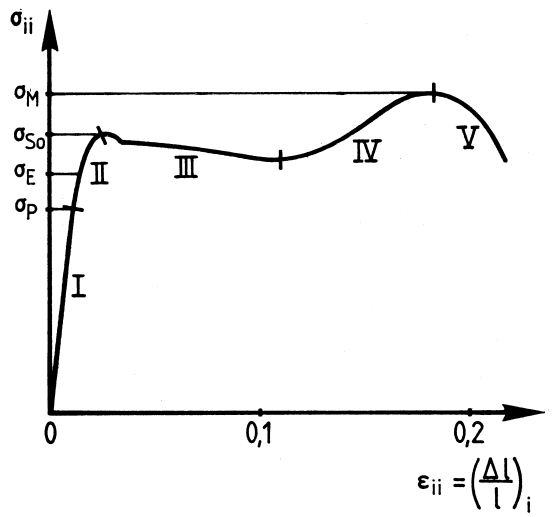

Figure 6.1 Typical stress–strain curve of a cylinder during uniaxial tensile testing along e_i. I: Region of proportionality between stress and strain (Hooke's law), II: Deviation from Hooke's law (quasi-reversible deformation), III: Plastic flow, IV: Strain hardening due to plastic deformation, V: Yield. σ_p denotes the region of quasi-proportionality, σ_E the region of reversible elasticity, σ_{So} the upper elastic bound, at which flow processes start to occur, and σ_M the yield strength. σ_{ii} relates to the cross-section of the cylinder without strain.

Physical Properties of Crystals. Siegfried Haussühl.

ISBN: 978-3-527-40543-5

We want to discuss the application of some important strength properties in more detail. We divide the strength properties roughly in the following domains:

1. Resistance against elastic deformation (elastic strength),
2. Resistance against plastic deformation (hardness),
3. Breaking strength.

The definition of elastic properties and their measurements was discussed in detail in Section 4.5.2. The question, to what extent elastic properties co-determine other strength properties, effective under totally different auxiliary conditions, will be answered in the following.

6.1.1 Hardness (Resistance Against Plastic Deformation)

Eminent technological importance is attached to plastic deformation processes not only in the processes of forming of workpieces, but also in those processes resulting, for the most part, in undesired changes of form during loading. It is therefore understandable that for a long time a focal point of research activities in industrial laboratories was dedicated to the clarification of these properties, resulting in the meantime, in the extensive literature on the subject. Here, we can only discuss some fundamental aspects which should make it easier to understand the phenomena. A first access to plastic deformation is provided by experience with highly viscous fluids, which can take on given forms under the influence of external mechanical forces. Here, the important thing is the time progression of the deformation and expenditure of deformation work. The latter can be assumed unmeasurably small in ideal fluids. As a measure of the deformation resistance of the viscous fluid, however, not the only reasonable one, one can use the dynamic shear resistance which must vanish in ideal fluids. The measurement of the propagation velocity v_T of a transverse wave of sufficiently high frequency (for example, higher than 10 KHz) yields the frequency dependent shear resistance of the viscous fluid $c_{44} = \rho v_T^2$. where ρ is the density. In any case, with fast loading, we expect a certain correlation between c_{44} and the viscosity and with resistance to plastic deformation. With quasistatic, that is, very slow loading we observe, even in highly viscous fluids, a vanishing c_{44}. These properties are impressively demonstrated by elastomeric materials, which behave like rubber under fast loading and like plastic clay under slow loading.

When we now carry over these ideas formed from practical experience to crystals, we expect that under low loading conditions plastic deformations only then appear on an easily measurable scale, when loading occurs slowly

and the crystal in question, possesses a very small shear resistance. This is at least qualitatively observed. However, if one compares different materials with approximately the same shear resistance, as, for example, silver chloride (AgCl) and potassium alum ($KAl(SO_4)_2 \cdot 12H_2O$), just to mention two familiar types of crystal, one finds extreme differences in resistance to plastic deformation. Crystals of silver chloride are almost "soft as butter." They can be easily deformed and bent. In contrast, an alum crystal offers a power of ten higher resistance to plastic deformation. It breaks like glass before appreciable deformation sets in. The reasons are of a structural nature.

It has been long known that morphological changes on the surface of crystals accompany deformation. This involves parallel grooves- or step-like recesses given the name *glide lines*. It was found that these lines could be understood as intersections of certain preferred lattice planes with the crystal surface. In such instances plastic deformation progresses via a parallel displacement of complete crystal layers parallel to the given planes as with the deformation of a stack of paper sheets or a book parallel to the pages. Furthermore, it was found that the deformation within these planes takes place in distinct directions, the so-called *glide directions*. Hence, such processes were characterized by two crystal-geometric quantities: *glide planes* and glide directions, together referred to as a *glide system*. If external mechanical stress is so applied that strong shear components appear in a glide direction, then plastic shear is easily effected. If several glide systems exist, as, for example, in cubic crystals, then several glide processes can simultaneously lead to a complicated deformation. Table 6.1 presents the glide systems for a few structural types.

Twin formation can also participate in an essential way in the deformation process. This involves the twinning of individual domains of a single crystal, which sometimes can take on macroscopic proportions under the influence of external stress. A long known example is twinning in calcite by uniaxial pressure approximately along one of the three long space diagonals of the rhombohedral elementary cell (Fig. 6.2). The achievable deformation is considerable. It results from the angle the individual twins seem tilted compared to the initial position. These kinds of twin formation can be produced in many crystals under appropriate stress conditions. The geometric details of twin formation are best investigated using X-ray methods (for example, the Laue method).

There exists a range of crystals which form twins even under extremely small mechanical stresses. Belonging to this class are, in particular, the ferroelastic crystals, which in a certain temperature range below the ferroelastic phase transformation often assume different twinning orientations even under weak finger pressure. This phenomenon does not appear in the temperature range above the transformation (prototype). Especially well suited for demonstration purposes are Sb_5O_7I (Nitsche et al., 1977) and $Rb_2Hg(CN)_4$ (Haussühl, 1978). A classification of the ferroelastics on the basis of the possi-

Table 6.1 Glide systems in some selected crystal types. The structure types are denoted according to the structure report (Ewald & Hermann, 1930). Glide planes are usually densely-packed lattice planes which appear morphologically as major growth planes. The glide directions are almost always along densely-packed lattice directions.

Structure	Examples	Glide plane	Glide direction
Face-centered cubic (A1)	Cu, Ag, Au, Pb	$\{111\}$	$\langle 1\bar{1}0\rangle$
Face-centered cubic (A1)	Al, Pt	$\{001\}$	$\langle 110\rangle$
Body-centered cubic (A2)	α-Fe, Mo, Nb, W	$\{011\}$	$\langle 1\bar{1}1\rangle$
Diamond (A4)	C, Si, Ge	$\{111\}$	$\langle 1\bar{1}0\rangle$
Zinc blende (B3)	ZnS, GaAs, InSb	$\{111\}$	$\langle 1\bar{1}0\rangle$
NaCl (B1)	Alkali halides of NaCl type; MgO, PbS	$\{110\}$, $\{001\}$	$\langle 1\bar{1}0\rangle$
CsCl (B2)	Alkali halides of CsCl type (CsCl, CsBr, CsI); TlCl, TlBr, NH_4Cl, NH_4Br	$\{110\}$	$\langle 001\rangle$
Fluorite (C1)	CaF_2, BaF_2	$\{001\}$	$\langle 110\rangle$
Calcite	$CaCO_3$, $NaNO_3$	$\{1\bar{1}1\}^*$	$\langle 110\rangle$
α-Quartz (C8)	SiO_2	$(001)^*$	$\langle 110\rangle$
		$\{100\}$	$[001]$
Baryte	$BaSO_4$, $KClO_4$	(001)	$[100]$
Gypsum	$CaSO_4 \cdot H_2O$	(010)	$[001]$

* Trigonal-hexagonal arrangement.

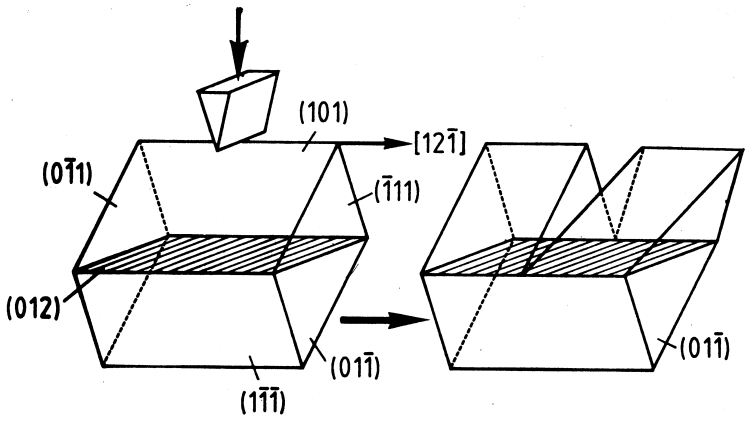

Figure 6.2 Example of twin formation in a calcite rhombohedron induced by uniaxial pressure perpendicularly to $[12\bar{1}]$. All indices refer to a trigonal-hexagonal setting. $[12\bar{1}]$ is the glide direction, (012) the glide plane which becomes also the twin plane. Therefore, only a discrete amount of gliding ist possible.

ble combinations of point symmetry of prototype and ferroelastics was given by Aizu (1969). Similar to the usual twin formation caused by pressure, a further deformation after twinning requires overcoming a new much higher resistance threshold.

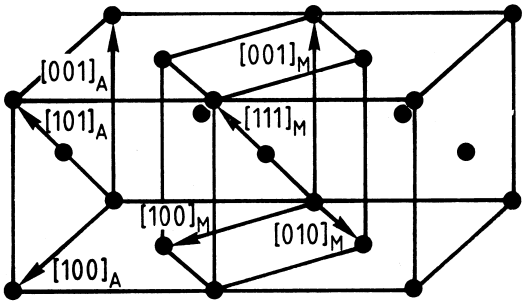

Figure 6.3 Position of the martensitic elementary cell in the austenitic lattice. The transition ist accompanied by the following changes in the interatomic distances: $a_{1,M} = 1.12a_A\sqrt{2}/2$, $a_{3,M} = 0.80a_A$. This results in an increase in volume of about 4%. In the $[111]_M$ directions, the interatomic distances remain virtually unchanged as compared to austenite, and $[111]_M$ is approximately parallel to $[101]_A$. (M and A denote martensite and austenite, respectively).

In some crystals, one observes plastic deformation coupled with a *phase transformation*. Such processes are favored when the transformation temperature is strongly dependent on the external mechanical stress; especially uniaxial pressure. At the working temperature of the deformation the crystals are then already in the region of instability or, the mechanical stress facilitates the start of the transition kinetics or even initiates them. Many ferroelastic crystals in the nonferroelastic high temperature phase belong to this category. Another long known and technologically very important type in this category is represented by the martensite transformation in the cooling of austenite (iron with a carbon content of over 0.1 % by weight; the iron atoms form a face-centered Bravais lattice) in martensite (the iron atoms form a tetragonal body-centered Bravais lattice). The transformation occurs only under a slight displacement of the lattice particles (Fig. 6.3). The phase transformations NaCl type → CsCl type or monoclinic ZrO_2 → tetragonal ZrO_2 (rutile type) and numerous transformations of alloys also belong to this category. Such a deformation leaves strong mechanical stress inhomongeneities in the deformed region which are coupled to an increase in mechanical strength. In many cases, the deformed regions spring back to the initial phase after a temperature increase, whereby the original shape of the crystal is restored (shape memory). The required threshold values for mechanical stresses and temperatures can, in most cases, be varied within a wide range by the addition of slight amounts of impurities. Hence, one can, for example, adapt the strength properties of steel to specific requirements.

We now want to dwell briefly on the mechanism of plastic deformation in the micro-range. The process of plastic shear along a glide plane demands a roll-off of atoms of neighboring lattice planes on top of one another. The critical resistance is found to be about a third of the corresponding shear re-

sistance from simple model calculations using spherical particles. The actual observed critical values for the onset of plastic deformation, the so-called critical flow stress, lies, however, several orders of magnitude lower. A qualitative understanding for this enormous discrepancy is found first in the close study of lattice defects, in particular, dislocations. These defects mostly originate in crystal growth as a consequence of unavoidable inhomogeneities (chemical composition, temperature).

Dislocations play a decisive role in plastic deformation. As shown by simple model calculations, dislocations can be made to move with far smaller mechanical shear stresses than the critical shear stress of the defect-free crystal, hence enabling a glide process. The resistance (Peierls potential) inhibiting the movement of the dislocations is overcome because only small pieces of the respective dislocation line stay in the domain of higher potential (kink formation), while the remaining dislocation line ends in potential wells (Peierls valley). Thus, the required threshold stress for plastic deformation is extremely reduced. A further condition is natural that a sufficient number of dislocations are available which do not interfere with one another in their ability to move. In the meantime one knows several mechanisms to generate dislocations with low energy expenditure as, for example, the Frank–Read source. The required activation energy depends essentially on the binding properties of the lattice particles. This explains the large variation of plastic properties in crystals with similar elastic properties. If, in the course of the formation of new dislocations under strong plastic deformation, a build-up of dislocations of various orientations takes place, then this can lead to an increase in resistance against further deformation due to the mutual interference of movement (*hardening*). These fundamental results were backed up by observations of dislocation structures before and after deformation with the aid of optical etching experiments, electron microscopy and X-ray topography. In few cases one could even make visible the movement of dislocations directly in the electron microscope.

The time progression of plastic deformation can be described to a first approximation by the change in the components of the deformation tensor with respect to time:

$$\frac{d\varepsilon_{ij}}{dt}.$$

If one assumes an approximately linear relationship between the components of the stress tensor and this deformation velocity, one would expect the following:

$$\frac{d\varepsilon_{ij}}{dt} = H_{ijkl}\sigma_{kl}(t).$$

Because of the complicated directional dependence of the plastic deformation process, which is not coupled in a simple way to the elastic anisotropy, H_{ijkl} cannot be freely interpreted as tensor components. Since plastic deformation of a probe in the ideal case (ideal plastic deformation), evolves under constant volume, we then have $\sum_i \varepsilon_{ii} = 0$ and hence, $\sum_i d\varepsilon_{ii}/dt = 0$.

However, due to the experimental difficulties involved to even measure good reproducible values with respect to this mathematical statement, it was only possible so far to collect data on cubic crystals, in particular, metals and alloys. According to practical experience, one expects, for the initial process of small plastic deformations, at most a certain possibility of a meaningful application of these formal tensor relations.

6.1.2 Indentation Hardness

The measurement of plastic properties on large single crystals in a macroscopic deformation experiment, for example, a tensile test, is comparatively expensive. Hence, for such a test it is advisable to employ a microscopic method which has been developed for perfection over a long time. It concerns the measurement of the so-called impression hardness. This involves pressing a diamond pyramid into the surface of the object. The resulting impression (so-called indentation), due to irreversible deformation, normally corresponds to a negative form of the diamond pyramid. From the dimensions, in particular, from the diameter of the impression, one can derive a quantity which, over a wide scale, turns out to be independent of the load of the diamond. The quantitative connection is as follows: In equilibrium, after the action of the diamond for a specific time, the resistance of the crystal against deformation absorbs just that force K loading the diamond. The resistance produced per unit area σ_0 is equivalent to the yield point. This means that the deformation would first advance after a further increase in load. The total resistance is equal to the area of the impression multiplied by σ_0; hence, $K = F\sigma_0$ with $F = Qd_{\text{eff}}^2$, where Q is the form factor of the pyramid and d_{eff} is a specific diameter. From this one obtains a measure for σ_0, the indentation hardness H,

$$H = \frac{K}{Q(d + d_0)^2},$$

where d_0 takes into account the elastic part of the deformation in equilibrium. Hence, $d = d_{\text{eff}} - d_0$ is the diameter of the impression after releasing the diamond. H as well as d_0 can be determined to amazingly good reproducibility after graphical evaluation of the measured values for different loads K and the associated diameters d. This involves plotting d as abscissa against $\sqrt{K}$. The gradient of the line of best fit yields $\sqrt{HQ}$ and hence H. The intersection of the line with the $\sqrt{K}$-axis ($d = 0$!) gives d_0 (Fig. 6.4).

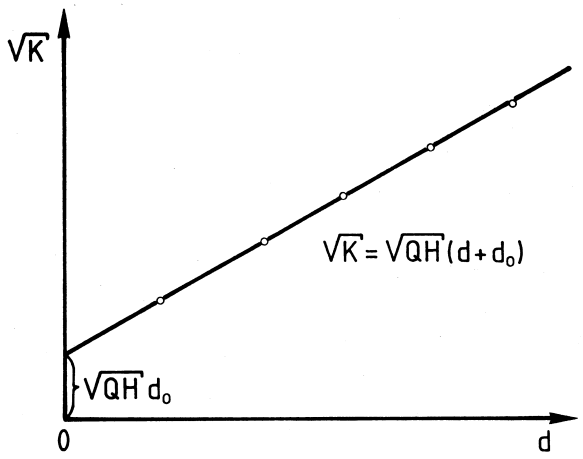

Figure 6.4 Graphical analysis of Vickers impression measurements.

In practice, the standard form of the diamond as a tetragonal pyramid with a height to base diagonal ratio of 1/7 (Vickers pyramid) has become widely accepted. If one measures the diagonal in micrometers, the applied force in Pond (1 kp = 9.807 N) and specifies H, the *Vickers hardness*, in kp/mm^2, the constant Q acquires the value $0.5392 \cdot 10^{-3}$. The Vickers hardness is then

$$H = 1854.4\, K/(d + d_0)^2 \quad (\mathrm{kp/mm^2}).$$

If the mechanical stress comes close to the flow stress as in the measurement of Vickers hardness, the plastic deformation does not come to a standstill, even after long observation times, due to continuous thermal activation. For this reason the loading time in these types of measurements must be limited, for example, to 20 s when measuring Vickers hardness. The method also allows hardness measurements on very small crystals with little time expenditure. Thus the method has proven itself as an analytical aid in qualitative phase analysis of coarse crystalline rocks, in particular, ores. A great advantage of the method is that only small areas on the surface of the crystals are damaged. The anisotropy of Vickers hardness in crystals is usually not very pronounced. In low-symmetry crystals, for example, gypsum or rhombic potassium nitrate, one observes not only different hardness values on different surfaces, but also surprisingly large deviations from the quadratic ideal form of the impression. Often, the size of the impression is dependent on the orientation of the diagonals within the surface of the test specimen. For example, most alkali halides display a smaller impression on (100) when the diagonal runs parallel to [011], and a larger one when it runs parallel to [001] (Fig. 6.5). From this, one can conclude that the glide system $(110)/[001]$ in these crystals has a larger share in the plastic deformation processes than the glide system $(100)/[011]$. In many

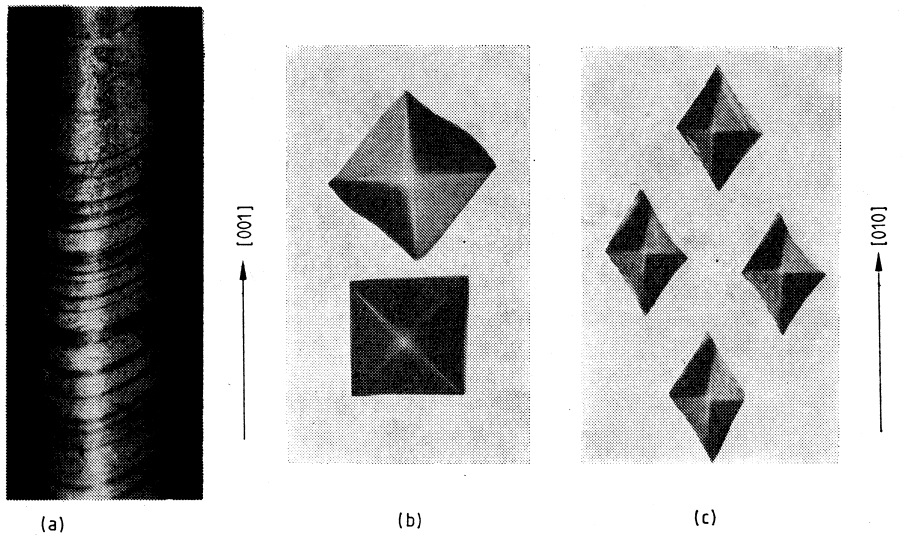

Figure 6.5 (a) Glide directions in a melt-grown Zn crystal (Bridgman–Stockbarger method). (b) Vickers impressions on a (100) surface in KCl. The minimum impression hardness is observed if the base edge of the pyramid is parallel $[011]$. (c) Anisotropic impressions on an (100) surface of KNO_3. The cross-sections of the impressions deviate markedly from a square.

cases a careful analysis of such details permits an insight into the kinetics of the deformation, which otherwise can only be obtained by rather tedious experiments. The use of diamonds with pyramid rhombic cross-section (Knoop pyramid) or other special forms can lead to further predictive statements in this field.

The investigation of Vickers hardness is especially easy to conduct with the well and comfortably equipped commercial units available today (micro hardness tester).

6.1.3 Strength

In contrast to plastic deformations, a breaking process is coupled with a substantial increase in the boundary surface. If one neglects the plastic deformation preceding the breakage, one expects that the energy expanded in the breaking process corresponds approximately to the energy required to create a new boundary surface. This also applies to a certain extent to glass fibres and to whisker-like crystals. Breaking processes can be initiated in macroscopic crystals with far lower energy. The reason is the existence of cracks and other inhomogeneities, which, in particular, considerably facilitate the initial

process of breakage, namely first crack formation. However, even under conditions of existing micro-cracks, the creation of the new boundary surface is the dominant principle. Consequently, a decrease in fracture work is expected when the boundary surface energy can be reduced, for example, by the absorption of surface-active molecules on the surface. Here we come across the phenomena, empirically investigated for hundreds of years, of the improvement of the effectiveness of tools by employing suitable liquids or sprays when drilling, milling, cutting, and grinding materials.

The experimental investigation of breaking properties in large single crystals is, just like the investigation of plastic deformation, an expensive exercise, which moreover, in single tests yields rather unreliable values. This is because normally the distribution of primary cracks and other so-called "notches" is not sufficiently known, except in those cases, where artificial crack systems are introduced. Fortunately, there exists a material property linked to breaking properties, namely abrasive strength, which is easily accessible to experiments and yields excellent, reproducible data. We will take a closer look at the two most important methods, which can also be used for the investigations on crystals provided they are of adequate size.

6.1.4 Abrasive Hardness

In the grinding process, the simultaneous action of sharp edges and corners of a great number of abrasive grains initiate numerous breaking processes on the surface. As a result, the surface is furrowed under a sometimes considerable fraction of plastic deformation, which can lead to hardening phenomena and finally to cracks and breaks with the formation of small particles. Their form and size depends on the grain size distribution of the abrasive as well as on the grinding liquid and of course decisively on the object itself. If one measures the loss in weight or volume of the object after a grinding process conducted under defined conditions, one finds a surprisingly good reproducibility of the abrasion. This mirrors the statistic character of abrasive hardness. Furthermore, it emerges that under otherwise similar conditions, the abrasion test over a wide range, independent of cross-section, is directly proportional to the force, with which the grinding tool presses against the specimen, as long as the abrasive does not possess too fine or a too coarse grains. An interpretation of this behavior turned out to be not quite simple. However, it is the prerequisite for the two most important methods to measure abrasive hardness . Kusnezow (1961) described in detail a method in which two crystals A and B are ground against each other and the ratio of the volume loss $V(A,B)$ is considered as a quantitative measure for the ratio of the abrasive hardnesses $F(A)/F(B)$. A closer study on calcium formate (Haussühl, 1963) showed, however, that the relation necessary to measure relative abrasive strengths

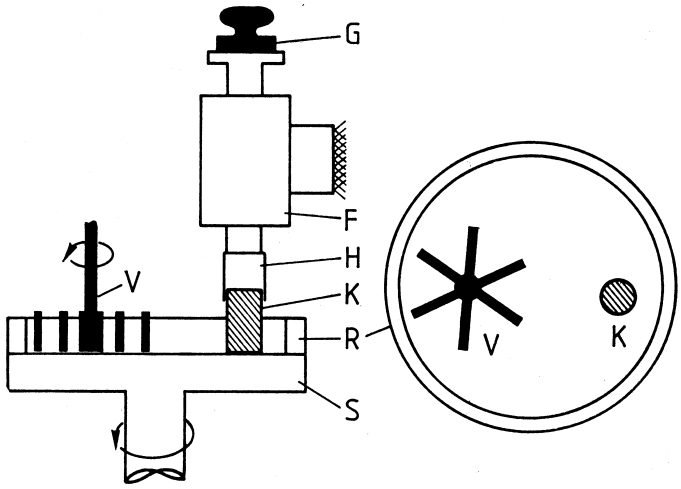

Figure 6.6 Illustration of the grinding apparatus according to v. Engelhardt und Haussühl. S Brass grinding plate with frame R, V abrasive distributor, K crystal with holder H, F bearing of crystal holder axis, G load.

using the *Kusnezow method*, $V(A,B)/V(A,C) = V(C,B)$, where A, B, C are three arbitrary crystal faces, is only approximately fulfilled (deviation under 1%), when the abrasive used possesses coarse granulation (about 100 μ grain diameter) or surface-active substances are added to the grinding liquid. The special advantage of this method consists of the low experimental expenditure and the fact that it is largely independent on secondary condition. The crystals are weighed before and after the grinding process; grinding pressure, grinding time and grinding motion have practically no influence on the measured result $V(A,B)$. NaCl (cubic faces) has proven quite useful as a reference crystal for soft crystals, while quartz (prism faces (100)) has proven as a reference for hard materials.

Another method used by Engelhardt and Haussühl (1960, 1965) to determine the abrasive hardness of many crystals allows the absolute measurement of the abrasive hardness under standardized conditions. Figure 6.6 shows a scheme of the equipment. The crystal, roughly machined to a cylindrical shape, is cemented in a holder to move freely in the vertical direction and pressed with a distinct weight G against the circular grinding plate. The distance of the axis of the crystal holder to the center of the grinding plate is 4 cm, so that the grinding path per revolution amounts to about 25 cm. The recommended standard conditions enabling a good reproducibility and comparability of the measured values are: rotational speed of the grinding plate: 24 revolutions/min; abrasive: high-grade corundum with a mean grain diameter of 140 μ ("Bikorit 100"); per test 10 g abrasive and 15 cm^3 grinding liquid;

100 revolutions at 100 g load on the crystal. More details are given in the cited work. A measure for the abrasive strength F is then the reciprocal of the abraded volume, hence, $F = V^{-1}$, where V is determined by the weight loss of the crystal after the grinding process.

By means of the considerations given below, we recognize a connection between the measured abrasive hardness F and the specific free boundary surface energy γ_i. This is the energy required to generate a boundary surface of the size of a unit area in the orientation denoted by the index i. The total mechanical energy E expended in the test is distributed over three parts: boundary surface work E_g, plastic deformation work E_p and frictional heat E_w. Hence, $E = E_g + E_p + E_w$.

We can formally specify the boundary surface work E_g as the product of a mean boundary surface energy γ with the total surface generated O: $E_g = \gamma O$. Using the simplification that the abraded particles possess the same form, we obtain $O = \alpha N^{1/3} V^{2/3}$, where α is a form factor and N is the number of abraded particles. Hence,

$$F^{-1} = V = (E - E_p - E_w)^{3/2} \alpha^{-3/2} \gamma^{-3/2} N^{-1/2}.$$

As an approximation, we further assume that the total applied energy E is constant in the standard grinding process. Furthermore, we expect that structurally related crystals do not exhibit too large difference with respect to E_p, E_w, α, and N. Thus, for such crystals, it is at least possible to make a qualitative estimation of the specific free boundary surface energy from the measurement of the abrasive strength. For two crystal types A and B it should be approximately $F_A/F_B = (\gamma_A/\gamma_B)^{3/2}$.

In particular, this allows an interpretation of the influence of boundary surface active liquids. For example, with alkali halides of the NaCl-type, one observes in pure xylol in a dry nitrogen atmosphere, an abrasive strength almost double as high as in a solution of 0.1 M stearic acid per liter xylol. Stearic acid turns out to be especially effective in reducing boundary surface energy just like, for example, certain amines as dodecylamine or other polar molecules. In order to obtain good reproducible values for abrasive strength it is advisable to use a sufficiently concentrated solution of polar molecules instead of a pure nonpolar liquid as a grinding liquid. Even the daily fluctuating values of air humidity can lead to changes in the measured values of up to several percent. These effects, however, can also be drawn to determine the relative boundary surface energy $\gamma_c' = \gamma_c/\gamma_0$. γ_0 and γ_c are the boundary surface energies opposing the pure liquid and opposing a solution of the polar molecules of concentration c (in M/l), respectively. With the aid of Gibbs adsorption equation

$$c_g = -\frac{c}{RT}\frac{d\gamma}{dc}$$

and the Langmuir adsorption isotherm

$$c_g = \frac{c_\infty c}{1/b + c}$$

one obtains the Szyskowski relation

$$\gamma_0 - \gamma_c = c_\infty RT \log(1 + cb).$$

where R is the universal gas constant, T is the absolute temperature, c_g and c_∞ are the concentrations and saturation concentration, respectively, of the molecules in the boundary surface and $b = ve^{L/RT}$, where v is the mole volume of adsorbed molecules and L is the adsorption energy of the molecules (per mole). If now one plots, instead of γ_c/γ_0, the ratio $(F_c/F_o)^{2/3}$ against the concentration c, the quantities c_∞/γ_0 and L by a best fit procedure and hence, gain information concerning γ_0 as well as the adsorption energy of the molecules on the given crystal. Full particulars are found in the work cited above (Engelhardt & Haussühl, 1960, 1965).

An overview of the general strength behavior of crystals is found in the diagram presented by Engelhardt and Haussühl (1965) in which the values for indentation hardness H (Vickers hardness) are plotted against the values of abrasive strength F, measured under comparable conditions (Fig. 6.7). This shows the expected relationship between the mechanical strength properties. The values of crystals of the respective isotypic series with fixed cation lie approximately on straight lines. The arrangement on these lines corresponds almost throughout to the sequence of the mean elastic resistance, expressed by the reciprocal volume compressibility K^{-1}. Crystals with very small shear resistances, for example, AgCl or KCN possess especially small hardness values in agreement with the models for plastic deformation discussed above. In contrast, crystals with low abrasive strength exhibit relatively large shear resistances. Interestingly, crystals of very low hardness, as AgCl or KCN exhibit comparatively high values of abrasive strength. This distinctive feature, also observed in the alkali halides, is certainly not solely due to the delayed effect of the plasticity on the breakage, but also due to the ability of such substances to adsorb grains on the surface during abrasion and hold these for a while, whereby, naturally an apparent increase in strength occurs. This is especially noticeable when using abrasives with fine granulation. Moreover, one finds that in the collective of crystals of approximately the same hardness, those with pronounced cleavage, i.e., with a distinct direction of especially low boundary surface energy, exhibit the smallest abrasive strength. In Fig. 6.7, the lines of approximately the same reciprocal compressibility run perpendicular to the main diagonals of the field. The distance of these lines from the zero point increases with increasing elastic resistance. The crystals located in the left and right outer regions of these lines are plastic or highly brittle substances, respectively.

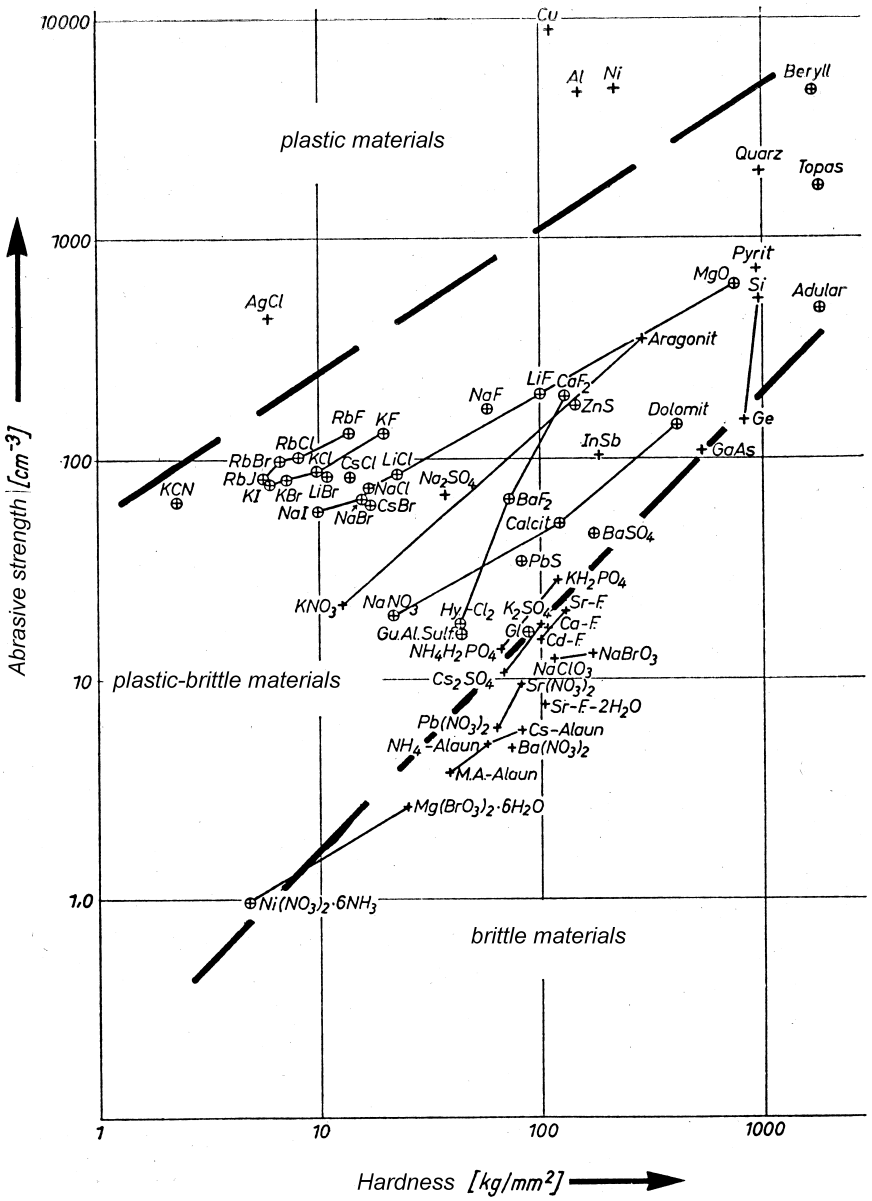

Figure 6.7 Abrasive strength vs. hardness diagram for different types of crystals in xylene after v. Engelhardt and Haussühl. Crystals with particularly low shear resistivity are denoted by ⊕. Abbreviations: $HyCl_2$ = hydrazinium dichloride, Gu.Al.Sulf. = guanidine aluminium sulfate hexahydrate, Ca-F., Sr-F., Cd.-F. = Ca, Sr, Cd formiate, M.A.-alum = methylammonium alum, Gl = triglycinium sulfate.

The numerous further strength properties, which play a role in materials science are naturally closely correlated with both the properties H and F discussed in this section. This also applies to the *scratch hardness*, used in qualitative mineral diagnosis. The *Mohs Hardness Scale* (actually scratch hardness scale) is a sequence of 10 minerals, whereby the one able to scratch the other is the harder of the minerals. There is no special order in which the scratch test is conducted. The hardness is measured on a scale from 1 to 10.

Talc	1	Apatite	5	Topaz	8
Gypsum	2	Orthoclase feldspar	6	Corundum	9
Calcite	3	Quartz	7	Diamond	10
Fluorite	4				

If, for example, a crystal scratched by apatite can scratch fluorite, it is given a Mohs hardness of 4.5. In practice, assigning such a number often causes difficulties because the scratch hardness on different faces also depends on the direction of the scratch in the face. Even scratching in one end in the opposite direction of a certain face can give widely different values, as, for example, with the mineral Disthen (Al_2SiO_5). A careful discussion of these properties is found in Tertsch (1949).

6.2 Dissolution Speed

The dissolution speed characterizes the ablation or etching behavior in a certain solvent. Whether the respective process is described by a physical solubility or a chemical dissolution is not important. The practical measurement is carried out as follows: A sufficiently large plane area of a crystal face is polished perpendicular to the direction $\boldsymbol{e}$. For all measurements, the diameter of the area should not be below a minimum value, for example 10 mm. A certain amount of solvent, say 100 g, is sprayed on the face of the crystal under fixed conditions, i.e., at a definite rate, fixed nozzle and equivalent flow conditions, fixed temperature and so on. An arrangement shown in Fig. 6.8 with the nozzle positioned close to the crystal face has been found to be satisfactory. Directly after the dissolution process the crystal is dried and the loss in weight is measured. This is a direct measure of the dissolution speed. The amount of solvent is so determined that not all-too deep dissolution furrows develop on the surface of the crystal. A proven method of evaluation is to plot the weight loss as a function of the amount of solvent in order to eliminate the expected influences due to the character of the surface as well as the wipe effect occurring independently of the amount of solvent used. The face

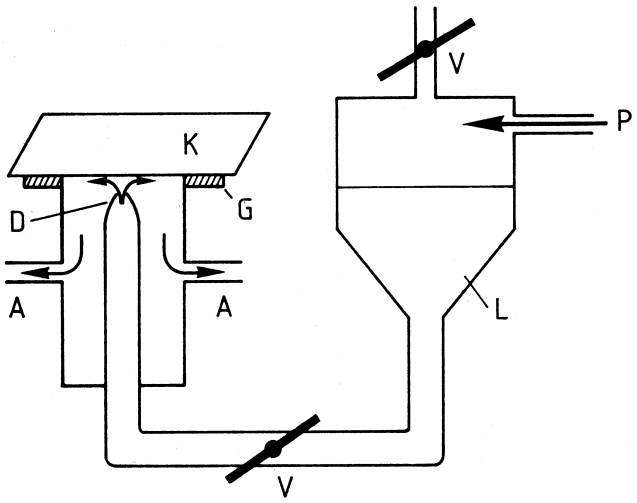

Figure 6.8 Arrangement for measuring of the dissolution speeds of crystals. K crystal plate facing the stream of solvent from the nozzle D with a circular area (diameter 14 mm). A drainage, L solvent, G rubber fitting, P pressurized air, V valves, distance between nozzle and crystal 4 mm, stream velocity 0.7 $\mathrm{m\,s^{-1}}$.

is to be polished anew for each individual measurement so that the same initial state is present. The gradient of the resulting straight line is a measure of the dissolution speed. A more detailed description of the measurement procedure and results is found in an investigation by Haussühl & Müller (1972). It is worth mentioning that the dissolution speed in directions $\boldsymbol{e}$ and $-\boldsymbol{e}$ can strongly differ when these directions, as in polar crystals, are not symmetry equivalent. Furthermore, one observes that already small additives in the solvent, of the order of a millionth, can effect extreme changes in the dissolution speed. These are often the same substances which in the growth of crystals influence crystal habit and produce a change in growth rate. In this respect, dissolution studies, which are simple and quick to carry out, can impart useful information on growth properties.

6.3 Sawing Velocity

Crystal sawing velocity has as yet received little attention and has hardly been investigated. Its measurement, as with dissolution speed, requires clear agreement as to the conditions to be kept. The respective object is in the form of a cylinder with the cylinder axis $\boldsymbol{e}$. It is advisable, however, not essential, to select a fixed diameter, for example, 10 mm for all measurements. The saw

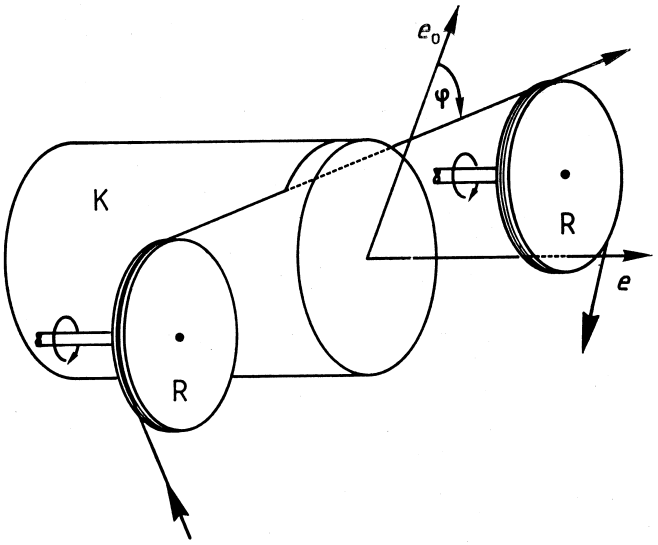

Figure 6.9 Measurement of sawing speed using a thread saw. The thread, uniformly wetted with a suitable liquid, runs with constant speed over the two wheels R. The cylindrical crystal K is pressed against the thread with a constant force. e is the normal to the cutting surface, e_0 a reference direction within the cutting surface.

thread, usually a nylon thread or a wolfram wire with a diameter of about 0.2 mm is guided with a constant velocity perpendicular to the cylinder axis, whereby the crystal is pressed against the thread with a given force. During the slicing process, the thread is evenly tensioned and wetted with a suitable liquid. The thread in advance of the crystal should be freed of excessive liquid with the help of a sponge. One measures the time required to cut through the cylinder at a fixed angle φ between the cutting direction and a reference direction e_0 (Fig. 6.9). The reciprocal value of the time multiplied by the surface correction factor πR^2 (R is the radius of the cylinder) gives the sawing velocity in mm^2/s. With soluble crystals one preferably uses suitable solvents as the lubricant and with metals, hardly soluble carbonates and silicates, one uses diluted acids or a suspension of abrasives in a viscous oil. For each cylinder orientation e one determines the dependence of the sawing velocity on the angle φ. The values for each e are plotted in the form of an even curve, whereby the position of e_0 is marked. A large number of such reference curves is required for the complete representation of the directional dependence. Here, it is also interesting that by reversing the sawing direction in certain low symmetry crystals, a change in the sawing velocity is observed.

6.4 Spectroscopic Properties

Most of the macroscopic properties discussed so far describe the behavior of homogeneous regions of a volume under the action of inducing quantities. A further group of properties, which are not directly representable by tensors, can be collected under the term *spectroscopic properties*. These are based on the interaction of photons or other particles or quasiparticles with the particles of the crystal lattice and the possible excitations resulting from these. We speak of spectroscopic properties in the narrow sense when the interaction is strongly dependent on the frequency or energy of the given radiation. For example, the propagation velocity of electromagnetic waves in crystals is weakly frequency dependent, the absorption in certain frequency ranges, however, is strongly frequency dependent. For a rough overview we distinguish between

(a) localized interactions or excitations of individual particles (electron states, nuclear states, vibrational, and rotational states)

(b) collective interactions tied to large undisturbed regions of the crystal (phonons, magnons, etc.).

In case (a) there appears characteristic differences to the interactions observed in free atoms or molecules. These are influenced by the binding of individual particles to neighboring particles and hence reflect the nature of the crystal field in the vicinity of the particles. Depending on the type of interaction, we understand under the notion "crystal field" the electric or magnetic field or the force field in the neighborhood of the given particle. The symmetry of the local crystal field, the so-called site symmetry, referred to the center of mass of the particle, is determined by a point symmetry group derived from the geometric space group symmetry at the given site. This shapes the finer details of the spectroscopic phenomena. Conversely, from such spectroscopic observations, one can make inferences on the crystal field and the interactions of the individual particles with their neighbors and hence on the binding resulting from such interactions.

As examples, we mention electron and nuclear spin resonance, nuclear resonance fluorescence (Mößbauer effect), high resolution X-ray fluorescence spectroscopy and optical spectroscopy, in particular infrared spectroscopy for the analysis of intramolecular vibrational states as well as Raman spectroscopy.

The effective crystal field is represented with the help of symmetry matched spacial functions. For example, the spacial change of the electric field is described to a first approximation by the tensor of the electric field gradient

$$Q_{ij} = \frac{\partial E_i}{\partial x_j} = -\frac{\partial^2 U}{\partial x_i \partial x_j},$$

where U is the electrostatic potential. More precise information on the tensor of the electric field gradient can be gained with the help of the Mößbauer effect when investigating certain types of atoms in crystals whose resonance absorption exhibits a particularly high sensitivity with respect to the action of the crystal field, as for example, ^{57}Fe. An analogous situation applies for electron and nuclear spin resonances and for the fine structure of the X-ray fluorescence radiation.

The collective vibrational states mentioned in case (b), that is phonons, magnons, and so on and their frequency distribution, i.e., energy distribution, are principally acquired through scattering and diffraction experiments using X-ray and neutron beams. An important aim in these investigations is the complete determination of the dispersion curves, i.e., the relationship $\lambda(\nu)$ between wavelength and frequency for different propagation directions and vibrational forms (modes) in the crystal. Complete knowledge concerning these properties has as yet only been achieved in crystals of high symmetry.

The interpretation of the spectroscopic observations mentioned in this section is based on a very essential manner on the symmetry properties of the crystal under investigation. Group theoretical methods have proven themselves especially for the classification and allocation of the states.

We refer the interested reader to the rich literature available not only on experimental spectroscopic methods, but also on crystal–chemical discussions of the spectra.